Available online at www.sciencedirect.com

SciVerse ScienceDirect

Journal of the European Ceramic Society 32 (2012) 579–588

www.elsevier.com/locate/jeurceramsoc

Mechanical behaviour of the constituents inside carbon-fibre/carbon-silicon carbide composites characterised by nano-indentation

Andy Leatherbarrow, Houzheng Wu *

Department of Materials, Loughborough University, Leicestershire LE11 3TU, UK

Received 10 June 2011; accepted 28 September 2011
Available online 22 October 2011

Abstract

The Young's modulus, hardness, fracture toughness and ductility of the key constituents were characterised using nano-indentation for three types of carbon-fibre/carbon silicon carbide composite manufactured through different routes and/or using different carbonaceous raw materials. Under indentation, all of the carbon constituents demonstrated much less ductile deformation than the silicon carbide and silicon did in these composites. Between two types of PAN-based carbon fibre, as well as of pyrolytic carbon, a difference of around a factor of two was evident in the Young's modulus and hardness. For the silicon carbide, a difference of around 100 GPa and 5 GPa was recorded for the mean Young's modulus and hardness respectively; for silicon, only a small variation was evident. The estimated mean fracture toughness of the silicon carbide ranged between 0.7 and 1.2 MPa.m$^{1/2}$, whilst the silicon was approximately 0.6 MPa.m$^{1/2}$. Results for the constituents were discussed in terms of their elastic/plastic behaviour.

Keywords: B. Composites; B. Fibre; C. Mechanical properties; D. SiC; Nanoindentation

1. Introduction

Carbon-fibre reinforced silicon carbon (C_f/SiC) and similar carbon fibre reinforced carbon-silicon carbide (C_f/C-SiC) composites are now well-established materials known to possess excellent tailorable and damage tolerant properties in comparison to monolithic ceramics.[1–3] These composites are manufactured by either liquid or gas phase routes as reviewed elsewhere[4–6] or alternate derivatives.[7–11] In recent years, liquid phase processing such as liquid silicon infiltration (LSI) has been gaining in popularity due to its rapidity and improved economy in comparison to the more established gaseous phase routes such as chemical vapour infiltration (CVI).

One of the key interests for these composites should be their application in friction brakes used in transport vehicles and heavy-duty machines. The tribological characteristics of C_f/C-SiC composites, in particular the coefficient of the friction (COF), COF stability and wear resistance are the key engineering performance properties that have been the focus of composites manufacturers, brake designers and suppliers, vehicle/machine manufacturers and of course end-users. Under specific friction conditions, such as during the run-in or bedding-in stage, under wet or excessive duty conditions, the tribological performance might become unfavourable. Therefore, tailoring of the friction couple is normally required: this includes the composites for the rotors and the lining materials for the pad.[5,12–16] From these investigations, it was agreed upon that the development of a friction transfer layer and premature damage in all scales on the surface of the composites influenced the friction performance.[16,17] The development of this so-called friction transfer layer should be based on the chemical interactions amongst the constituents embedded inside the friction couples, whilst its longevity should be inherently defined by the cohesion of the layer and the interface between the layer and the composite surface. Therefore, considering the brittleness of the ceramic constituents in the composite, any fracture near the surface could be detrimental to the sustainability of this friction transfer layer; the presence of which is considered to be crucial to maintain a desired COF and its stability.[16,13]

It is well established that the load-carrying capability of the composite is defined by its macro-scale mechanical properties, such as the tensile or bend strength, fracture toughness

* Corresponding author. Tel.: +44 1509 223342; fax: +44 1509 223949.
E-mail address: h.wu2@lboro.ac.uk (H. Wu).

0955-2219/$ – see front matter © 2011 Elsevier Ltd. All rights reserved.
doi:10.1016/j.jeurceramsoc.2011.09.026

(or fracture energy) and elastic properties (Young's modulus, Poisson's ratio). However, fracture on the surface, particularly at the small scale should be dictated by the micro-scale properties. Therefore, the properties at this scale must be heavily weighted on the initiation of fracture damage. For highly heterogeneous materials like C_f/C-SiC composites, properties in micro-scales should include those of the carbon fibre (C_f), pyrolytic carbon (pyC), silicon carbide (SiC), silicon (Si), as well as the interfaces in between them. It is therefore, the focus of this paper to measure the mechanical behaviour of these constituents and also reveal if their behaviour is subject to any influence from the manufacturing conditions. In addition, these measurements might also provide additional information to further our understanding of any premature failure of the constituents at the friction surface during braking.

Endeavours to improve the manufacture of these composites may include the selection of a number of raw materials and processing routes. A range of carbon fibres could be incorporated as the reinforcing fibres, just as carbonaceous materials for production of the pyC could be included as part of the matrix, in addition to different sources of SiC. Carbon fibres are normally classified as PAN- or pitch-based, depending on the precursor source, being either polyacrylonitrile (PAN) or meso-pitch respectively. The carbon fibres are typically manufactured through a process of drawing, oxidising, carbonising, and further high temperature treatment to increase the carbon content, and size and quality of graphite crystallites that may improve or modify the physical and mechanical properties of the fibre.[18] Due to the differences in the quality of the precursors and processing conditions used, a range of PAN carbon fibres are available. These are normally categorised as high resistance (HR), intermediate modulus (IM), high modulus (HM) and ultra high modulus (UHM), according to their tensile modulus and strength along the fibre direction. However, there is a current lack of knowledge in the literature regarding what kind of carbon fibres would be best suited for improving either the mechanical or tribological properties of C_f/C-SiC composites.

PyC in the composite has several roles, both during LSI manufacture and in the load-carrying capability of the final composite. First, the pyC is the production source for the SiC when it makes contact with the Si melt or vapour.[19] Second, high density pyC is required to prevent the Si melt reacting directly with the carbon fibres. Thirdly, residual pyC between the carbon fibre and SiC is necessary to dissipate any fracture energy through the splitting of interfaces at the fibre/pyC and/or SiC/pyC, or cracking inside the pyC itself along the fibre direction, which leads to a direct consequence of halting catastrophic crack propagation. Currently, pyC is introduced on to the surface of carbon fibres through either pyrolysis of impregnated resins or deposition of cracked carbonaceous gases at high temperatures, known as polymer infiltration and pyrolysis (PIP) and CVI respectively. In a similar respect to the fibre selection, little is known about the impact of the pyC on the performance of the composites and the production of SiC, even though there exists a clear gap in the production cost and the nature of the pyC created by the PIP and CVI processes.

For more than a decade, nano-indentation has been widely used to characterise the mechanical behaviour of very small regions, which today ranges between around 500 nm to ~20 μm.[20–23] Due to the small indentation sizes, tiny loads are typically used between 20 and 250 mN, using a ball, three- or four-sided point of known geometry, such as the Vickers or Berkovich indenter. The hardness and Young's modulus for the SiC and Si phases inside these composites have already been reported.[24,25] However, the properties of the other phases, including the impact of the microstructural factors on the properties of the constituents have so far not been understood enough. This includes different types of carbon fibre and origins of carbonaceous matters used as the reaction source for the molten Si during LSI. In addition, the indentation fracture method has so far been used to generate indents with propagating cracks, and the lengths of which can be used to estimate the fracture toughness[26,27] using an equation introduced by Lawn et al.[28] Therefore, the fracture toughness of the constituents inside these composites can be estimated using nano-indentation. However, considering the differences in the scale of fracture, any estimated fracture toughness derived from nano-indentation measurements may only be appropriate to gauge the resistance of the crack initiation at the micro-scale; this is instead of directly comparing any measurement to macro-scale indentation test under much larger loads or alternatively, the single edge notched bending (SENB) test.

2. Experimental details

2.1. Sample preparation

Three different C_f/C-SiC composites were prepared comprising two types of carbon fibre and three types of pyC, apart from SiC generated through the same LSI process and any residual Si. Carbon fibres included PANOX carbon fibre, called PO C_f and AS4 PAN carbon fibres called AS C_f. The former is widely used in commercial carbon/ceramic composites, whilst the latter was acquired from a commercial source. The carbonaceous sources for the three types of pyC included methane, phenolic and epoxy resin. The manufacturing process of the composites is only highlighted here. First, carbon fibre/carbon performs (C_f/C) were prepared through the following routes: (i) pyC derived from methane was deposited around the PO C_f filaments and bundles through the CVI process; (ii) pyC derived from epoxy was wrapped around the AS C_f filaments and bundles through direct pyrolysis of the AS C_f pre-preg (Hexply, Hexcel Ltd, UK) where the matrix was epoxy resin; (iii) pyC derived from phenolic resin was wrapped around the AS C_f bundles through direct pyrolysis of AS4 C_f pre-pregs with phenolic resin (Hexcel Ltd., UK). The C_f/C preforms were then infiltrated with Si melt at a temperature of 1500 °C under a flowing argon atmosphere. The resulting C_f/C-SiC composites were ground and polished to a 1-μm diamond grit finish using polishing wheels (Struers, Tegra-pol, Denmark) and called CVI-C, Epoxy-C and Phenolic-C, based on the carbonaceous source used or the means

to introduce into carbon fibre architectures. More details on the manufacturing process are available elsewhere.[29]

2.2. Microstructure examination

An optical microscope (Reichert-Jung, MEF-3, Austria) was used to identify the indents using a combination of polarised and differential interference contrast (DIC) light to optimise the contrast between the phases and interfaces. A FEG-SEM (Carl Zeiss (Leo) 1530VP, Cambridge, UK) was used to image the indentations and any propagated cracks in the secondary electron mode at 5 kV. Meanwhile, image manipulation software (GIMP, USA) was used to estimate the length of any propagating cracks.

2.3. Nano-indentation measurements

A nano indenter (Micro Materials Ltd., UK) was used in conjunction with a Berkovich tip to generate indents inside the different phases of the C_f/C-SiC composites. The polished samples were glued on to a sample holder and placed inside a temperature and humidity controlled chamber. An optical microscope was used at 400× magnification to identify the location of each indent. At least eight indentations were performed in each phase using a force of 100 mN (unless otherwise specified) with a loading rate of 2.5 mN s^{-1}. The testing parameters were based on the power-law fit method from Oliver and Pharr in 1992,[20] which was updated in 2004.[21] The mechanical properties of the carbon fibre, pyC matrix, SiC and Si in each composite were investigated. Data collected included: maximum depth (h_{max}) at maximum load, final depth after fully un-loaded (h_f), maximum load (mN). The hardness, H (GPa) and reduced modulus of elasticity, E_r (GPa) were estimated using Eqs. (1) and (2) respectively.

$$H = \frac{P_{Max}}{A_r} \tag{1}$$

$$\frac{1}{E_r} = \frac{(1-\upsilon_i^2)}{E_i} + \frac{(1-\upsilon_s^2)}{E} \cdots \tag{2}$$

where P_{max} the maximum load (mN), A_r the projected area of contact and 'ν' is the Poisson's ratio. E_i and E are the Young's modulus for the indenter and the sample respectively, where for a diamond indenter tip, $E_i = 1141$ GPa and $\nu_i = 0.07$. The Poisson's ratio varies according indented phase and crystal orientation. The most common values of ν_s were chosen as follows: 0.23 for a typical AS4 carbon fibre (note: may vary from 0.20 (UHM) to 0.25 (UHS) for PAN-derived carbon fibre[30]); 0.27 for monolithic pyC,[31] 0.188 for SiC,[32] 0.27 for Si along [1 1 1] orientation.[33] The fracture toughness (K_{IC}) was estimated using the Berkovich indentation fracture method and equation (3)[28]:

$$K_{1C} = \delta\left(\frac{E}{H}\right)^{0.5} \frac{F_m}{c^{3/2}} \tag{3}$$

where E is the Young's modulus (GPa), H the hardness (GPa), F_m is the maximum applied force (mN), c the length of the crack path from the centre of the indent (μm) and δ an empirically determined calibration constant, taken as 0.016 for the Berkovich

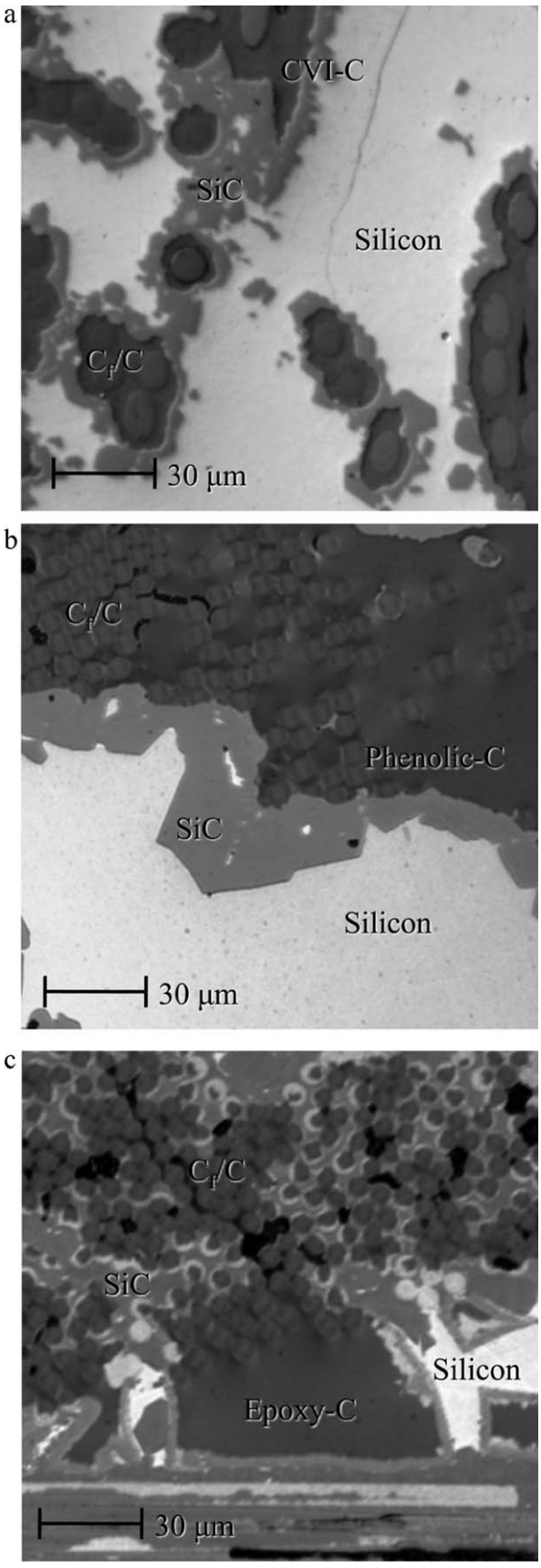

Fig. 1. Overview of the microstructure of each C_f/C-SiC composite imaged under polarised and DIC light conditions. (a) CVI-C, (b) Phenolic-C and (c) Epoxy-C.

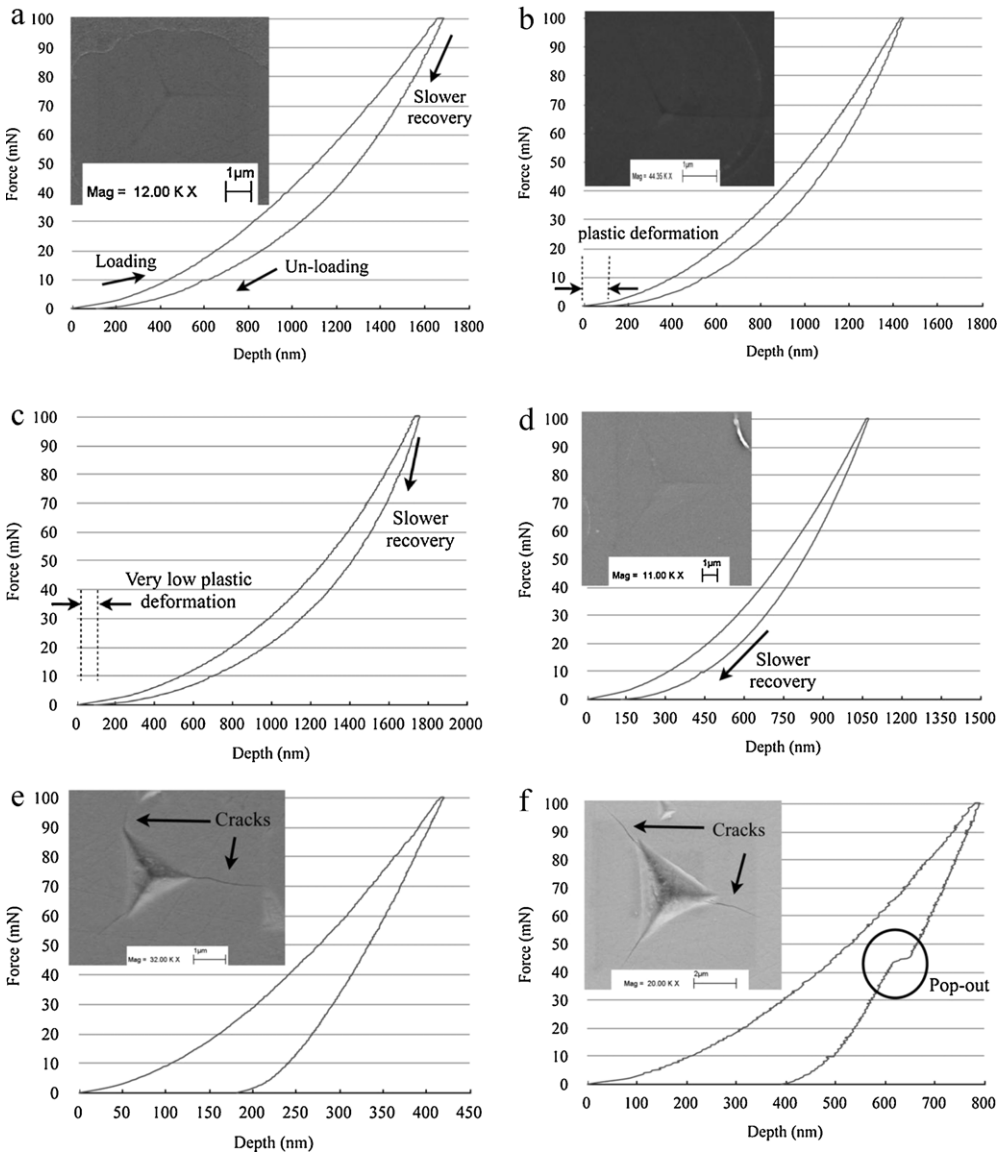

Fig. 2. Representative load-displacement loading and un-loading curves for the constituents inside the composites under a maximum indenting load of 100 mN. (a) PAN-OX carbon fibre in CVI-C, (b) PAN carbon fibre in Phenonic-C, (c) pyrolytic carbon in CVI-C, (d) pyrolytic carbon in Phenonic-C, (e) SiC in CVI-C, and (f) Si in CVI-C.

tip.[27] Any successful propagating cracks were imaged using optical microscopy, at magnifications up to 1000× and at higher magnifications using the FEG-SEM.

3. Experimental results

3.1. Microstructure of the composites

The representative microstructures for each composite are illustrated in Fig. 1. For all of the composites, the same hierarchal structure developed amongst the constituents. A layer of pyC wrapped around the carbon fibre filaments and bundles, which is commonly referred to as the carbon fibre/carbon (C_f/C) region. SiC and Si exists in amongst C_f/C regions, where the latter always surrounds the former.

The measured fibre diameters were approximately 9.1 and 7.1-μm for the PO C_f in the CVI-C and AS C_f in the Phenolic-C/Epoxy-C respectively. The thickness of pyC was approximately several micrometres, although could be much thinner or thicker depending on the location. The typical SiC layer thickness ranged between 1 and 30-μm, whilst the equivalent size of the Si lakes or pools could vary from the sub-micrometre up to hundreds of micrometres. More details on the microstructure of these composites are available in another paper.[29]

3.2. Characteristics of the force-displacement curves and indentation impressions

Fig. 2 shows the force-depth curves of the indentations, including FEG-SEM micrographs of the impressions inside the

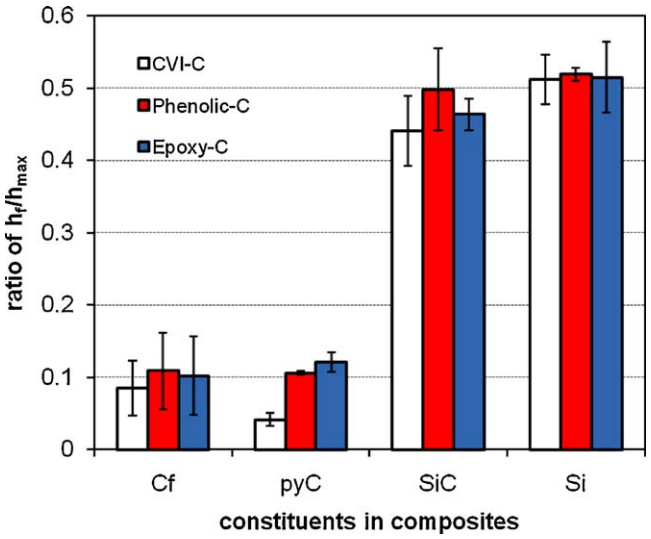

Fig. 3. The ratios of h_f/h_{max} in nanoindentation impressions of each constituent in the composites (Cf – carbon fibres, pyC – pyrolytic carbon, SiC – silicon carbide and Si – silicon).

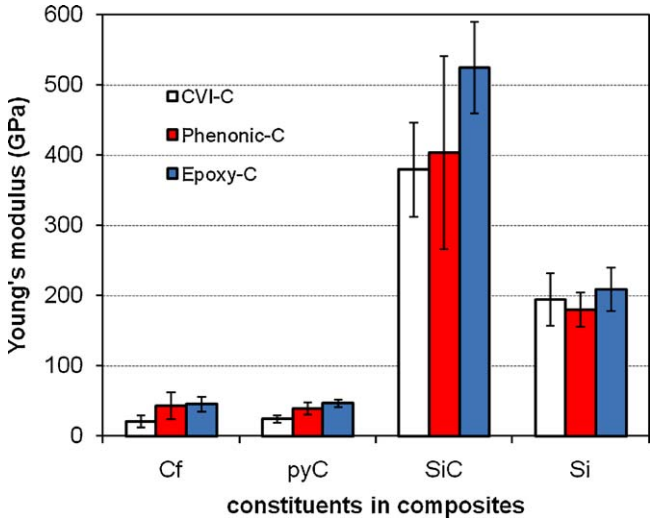

Fig. 4. Measurements of Young's modulus of each constituent in the composites (Cf – carbon fibres, pyC – pyrolytic carbon, SiC – silicon carbide and Si – silicon).

carbon fibres, pyC, SiC and Si. Judging solely from the visual shapes of the curves, there is a clear difference between the carbon (C_f and pyC) and ceramic (SiC and Si) constituents.

The ratio of the final depth of an impression, h_f, against the penetration depth, h_{max}, at the maximum load was extracted for each constituent in all of the composites. The results are summarised in Fig. 3. Between the two types of carbon fibre, the averaged ratios were just around 0.1. For the pyC, the ratio in the Epoxy-C and Phenolic-C was slightly over 0.1 and just 0.1 respectively, and in the CVI-C less than 0.05. For the SiC, it is apparent that the ratio in the Phenolic-C was slightly higher than those in other two composites. Meanwhile, there was no clear difference for the Si amongst these composites. Overall, the ratio for Si was slightly higher than the SiC, whilst both constituents possessed a much high ratio than the carbon constituents.

Apart from the pyC inside the CVI-C, FEG-SEM micrographs of the impressions from each constituent are included as an inset in each force-depth graph. There was no evidence inside any of the micrographs that the carbon fibres were pushed out, cracked or split under the current testing regime, neither was any cracking evident inside any of the pyC regions. Consequently, it was unfeasible to estimate the fracture toughness in any of the carbon constituents. In contrast, all of the SiC and Si phases readily cracked, which permitted the measurement of crack lengths so the fracture toughness could be estimated. According to the micrographs, there was no preferential location for the crack initiation. However, the cracks typically propagated from the corners of the indent, whilst some also originated from the sides.

3.3. Young's modulus

The Young's modulus results for each constituent are summarised in Fig. 4. The mean Young's modulus of the AS C_f was approximately double that of the PO C_f, whilst variations in the values for the AS C_f in the composites made from different resins was minimal. The Young's modulus of the pyC in the CVI-C was the lowest, and in the Epoxy-C the highest, with a difference of around a factor of 2. There was minimal difference between the Young's modulus of the pyC derived from phenolic and epoxy resins.

For the SiC, the mean value in the Epoxy-C composite was approximately 30% higher in comparison to the SiC derived from the CVI-C and Phenolic-C. However, the standard error in Phenolic-C was around two times larger than those in other two composites. Any observed differences in Young's modulus of the Si was limited, if any amongst the composites.

3.4. Hardness

According to the hardness results in Fig. 5, the AS C_f possessed a mean hardness of more than doubled in comparison to the PO C_f inside the CVI-C composite. There was only a minor difference in the composites derived from different resins,

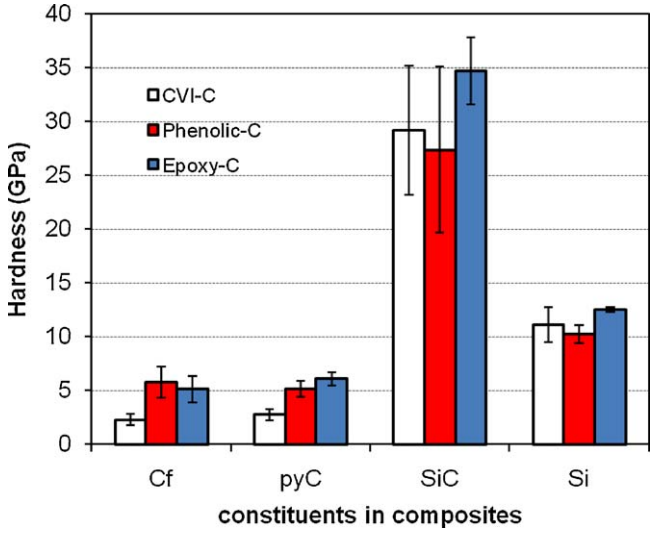

Fig. 5. Measurements of hardness of each constituent in the composites (Cf – carbon fibres, pyC – pyrolytic carbon, SiC – silicon carbide and Si – silicon).

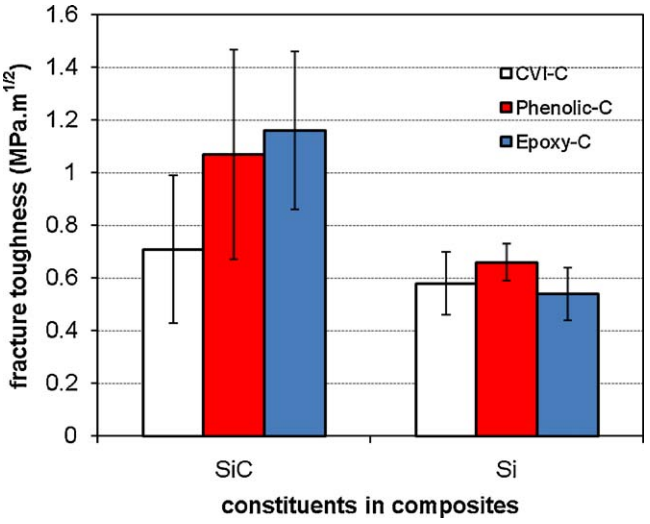

Fig. 6. Measurements of fracture toughness (K_{IC}) of each constituent in the composites (Cf – carbon fibres, pyC – pyrolytic carbon, SiC – silicon carbide and Si – silicon).

although standard deviation for AS C_f was significantly larger than that for the PO C_f. For the pyC, the hardness of these derived from resins was about 100% higher than that derived from methane via CVI process. It is noted that the pyC derived from epoxy was slightly harder than that from phenolic resin.

For the SiC constituents inside the CVI-C and Phenolic-C composites, the margin of the difference was small. With respect to the mean values and scale of the standard deviation, the hardness of SiC in the Epoxy-C was about 20% higher than those in other composites. By comparison, any differences for the Si were very small amongst these composites.

3.5. Fracture toughness

The estimated fracture toughness values are summarised in Fig. 6, which varied between approximately 0.71 and 1.16 MPa.m$^{1/2}$ for the SiC. The mean values of the SiC in the Phenolic-C and Epoxy-C were about 50% higher in comparison to the SiC inside the CVI-C. It was also noticed that the standard deviations of the SiC measurements were quite high, but not for the Si. The estimated toughness of which ranged between 0.54 and 0.66 MPa.m$^{1/2}$, with significantly smaller standard deviation; there was no clear difference amongst these composites.

4. Discussion

4.1. Factors affecting the Young's modulus and hardness of the constituents inside the C_f/C-SiC composites

Considering the turbostratic structure of pyC and PAN carbon fibres, one might consider to estimate the upper and lower bounds of Young's modulus of these carbons using constitutive relations for any randomly distributed polycrystals. In the pyC, the crystallites should all be hexagonal graphite. If any biased orientation of the graphite crystallites and possible existence of amorphous carbon are neglected, the upper bounds for bulk (B_v) and shear modulus (μ_v), also called Voigt bound, can be estimated using formula's Eqs. (4) and (5) respectively[34]:

$$B_V = \frac{2(C_{11} + C_{12}) + 4C_{13} + C_{33}}{9} \tag{4}$$

$$\mu_V = \frac{G^v_{eff} + 2C_{44} + 2C_{66}}{5} \tag{5}$$

The lower bounds, also called Reuss bounds, are given by the relationships in Eqs. (6) and (7):

$$K_R = C_{13} + \frac{(C_{11} - C_{66} - C_{13})(C_{33} - C_{13})}{C_{11} + C_{33} - C_{66} - 2C_{13}} \tag{6}$$

$$\mu_R = \left[\frac{1}{5}\left(\frac{1}{G^r_{eff}} + \frac{2}{C_{44}} + \frac{2}{C_{66}}\right)\right]^{-1} \tag{7}$$

where C_{ij} are the elastic components of hexagonal crystal; G^V_{eff} is the energy per unit volume in a grain when a pure uni-axial shear strain of unit magnitude is applied to the grain along its axis of symmetry,[34] which can be calculated from Eq. (8):

$$G^v_{eff} = \frac{C_{11} + C_{33} - 2C_{13} - C_{66}}{3} \tag{8}$$

G^r_{eff} is the energy per unit volume, in a grain when a pure uni-axial shear stress of a unit magnitude is applied to a grain along its axis of symmetry[34] which can be calculated using Eq. (9):

$$G^r_{eff} = \frac{K_R G^v_{eff}}{K_v} \tag{9}$$

where K_v=[2(C_{11}+C_{12})+4C_{13}+C_{33}]/9. For isotropic materials, the Young's modulus can be calculated using Eq. (10):

$$E = \frac{9\mu K}{3K + \mu} \tag{10}$$

The single crystal data for graphite used here were based on Berryman's quotation,[35] where C_{11} = 1060 GPa, C_{12} = 180 GPa, C_{13} = 15 GPa, C_{33} = 36.5 GPa and the value of C_{44} is well known for its uncertainty. Whilst the value of C_{44} has little influence on the value of the estimated upper bounds, it does significantly influence the value of the lower bound. The estimated bounds of the Young's modulus are therefore plotted against the possible values of C_{44}, as shown in Fig. 7. The mean Young's modulus, measured by the nano-indentation of the carbon constituents is represented by the dashed horizontal lines in Fig. 7. Clearly, the Young's moduli measured by nano-indentation are well below the estimated upper bound and tend to hit the lower bounds instead.

It is yet unclear why the Young's modulus measured by the nano-indention tends to hit the lower bounds. As it is known, the Voigt upper bound is also called the isostrain average; it gives the ratio of the average stress to average strain when all of the crystallites are assumed to have the same strain. The Reuss lower bound is sometimes referred to as the isostress average; it gives the ratio of average stress to average strain when all of the crystallites are assumed to have the same stress. For an isostrain condition, it requires a parallel loading condition along the parallel direction of the "rigid" and "soft" constructional

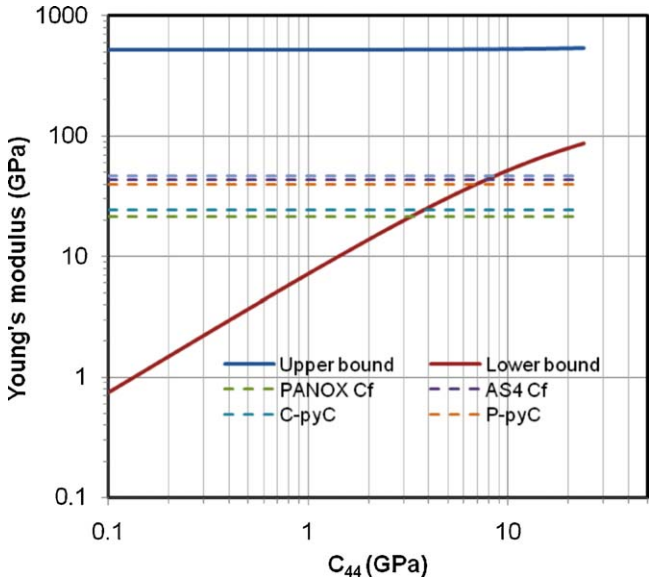

Fig. 7. The estimated bounds vary with the shear component of graphite crystal for graphite polycrystal with randomly distributed graphite crystallites. The dashed lines show where the measured levels by nanoindentation were of Young's modulus of carbon constituents in the composites.

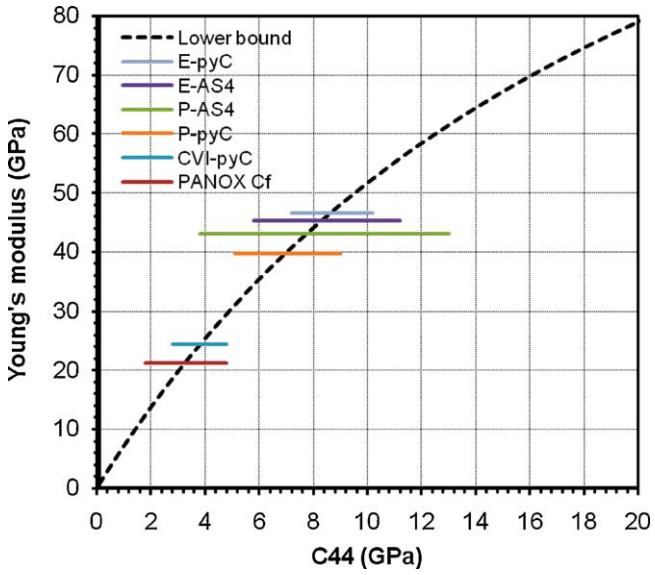

Fig. 8. The C_{44} readings for each carbon constituent in the composites. The dashed line is the estimated lower bounds of Young's modulus in polycrystalline graphite.

components. Meanwhile, for an isostress condition, the loading direction needs to perpendicular to the parallel direction of the "rigid" and "soft" components. Therefore, when most of the basal planes of the graphite crystallites are aligned along the fibre direction, the stressing condition around the indenter inclines to provide an isostress condition along the transverse direction, when indenting is along the longitudinal direction of the fibres. Consequently, the Young's modulus measured by indentation should be closer to the lower bond.

Using the measurements of the Young's modulus and the lower bound curve in Fig. 7, we can read the mean "C_{44}" value for each carbon constituent. The estimated range of C_{44} is presented in Fig. 8, with each corresponding mean Young's modulus value. The C_{44} for both the fibre and carbon matrix in the CVI-C composite ranges between 2 and 5 GPa. For the AS C_f and pyC derived from the resins, the C_{44} is larger than 5 GPa, ranging up to and beyond 10 GPa.

C_{44} is the shear modulus between the basal planes. According to Kelly,[36] the most reliable value of the modulus for basal plane shear in graphite free of disorder should be 4–5 GPa. The modulus decreases as the amount of imperfection increases; therefore the range can vary widely depending on the quality of the carbon, which could be dictated by the number of defects between the graphene layers. It was noticed that the C_{44} value of graphite was improved by γ irradiation, although other elastic components barely changed[37]; this is because the irradiation reduced the basal dislocations. However, little support for this can be found from the selected area diffraction (SAD) patterns where pyC and PO C_f in CVI-C had the smallest $d_{(002)}$, i.e. a better graphilisation than others.

Whilst the derived C_{44} values for the AS4 is larger than the theoretical values, these values are closer to the estimated C_{44} for the PAN carbon fibre using the uniform stress model, a model that was used to estimate the Young's modulus in fibre direction.[38] Therefore, it may be possible that nano-indentation could become a method to estimate the C_{44} value, a key parameter to predict the mechanical property of carbon fibres based on the current models, if the estimation could be further justified.

4.2. Factors that affect the hardness of the constituents

The ratio of h_f/h_{max} indicated that all carbon constituents in the composites exhibited a much lower ductile deformation, if any. Therefore, the pyC could be approximated to perfect elastic solids. Based on the concept of an effective indenter, proposed by Pharr et al.,[39] if the ratio is close to zero, there would have little ductile deformation around the indenter developed. Therefore, the indentation pressure is a direct measure of the elastic property of the carbon and therefore should abide to the relationship in Eq. (11) with Young's modulus, $E/(1-\nu^2)$, of carbon and the semi-apical angle θ of the indenter:

$$P = H = 0.5\left(\frac{E}{1-\nu^2}\right)\cot\theta \tag{11}$$

From Fig. 9, even though the measured hardness exhibited a difference of up to a factor of 2 amongst the carbon constituents in these composites, a linear relationship was indeed seen between the averaged H and E values. However, note the relatively large standard deviation that exists for both E and H and the data for AS4 C_f in Epoxy-C that slightly departed from the linear line.

For the SiC and Si, the ratios of h_f/h_{max} are between these for perfect elastic and plastic solids. They should therefore belong to the category of elastic-plastic or elastic-brittle solids. Whilst ceramics are normally treated as elastic-brittle solids, we have little reason to exclude ceramics like SiC and Si as elastic-plastic solids under the condition of nano-indentation. This is because ductile deformation around the indentation does exist in these

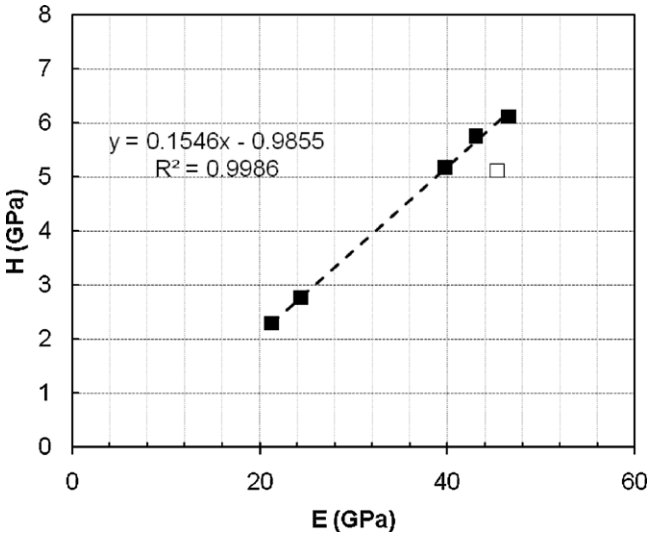

Fig. 9. Linear relationship between the measured hardness and Young's modulus for all carbon constituents in the composites.

constituents. An additional point to consider is that our nano-indentation was performed under much smaller load than typical micro-indentation. These smaller loads likely lead to a heavier weight of any ductile deformation underneath the indentation in comparison to cracking, if any. If the SiC and Si are elastic-plastic solids under these nano-indentation conditions, the mean contact pressure, i.e. the hardness, should be defined in Eq. (12) as the yield stress, Y:

$$H = \sim 3Y \tag{12}$$

This critical yielding stress is defined by the critical shear stress of dislocation motion. For such a dislocation motion based yielding, work hardening likely appears during indentation. Therefore, the Hall-Petch law should be applicable in these materials, i.e. the reduction of grain size increases the yield stress. Amongst the composites, TEM images showed that the grain size of SiC in Epoxy-C composite was smaller than that in CVI-C and Phenolic-C composites.[29] This might explain why the measured hardness in the Epoxy-C was the highest. Our TEM studies also showed that nano-sized SiC region existed in the side near the pyC in all of the composites; the scales of which in the CVI-C and Phenolic-C were much smaller than that in the Epoxy-C,[29] where the CVI-C possessed the smallest nano-sized SiC region. It is also this coexistence of the nano-sized and micro-sized SiC regions that might have contributed to the large scattering of the measured hardness results in the composites. In the Si regions, the hardness values were very similar and significantly less scattered. Presumably, all of the Si regions in the composites should have the same microstructure as they were crystallized from the same melt under the same history.

4.3. Crack initiation resistance

For single crystal Si, cracking normally occurs along the <1 1 1> cleavage planes, where according to Ericson et al.,[40] the fracture toughness varied between 0.83 and 0.95 MPa.m$^{1/2}$ along this direction. The values reporter in this study for the Si in all three composites were lower, but close to the values measured for a single crystal of silicon. This similarity might be explained by the fact that the size of the Si crystallites in the Si pool are generally much larger than the sampling size of the nanoindentation used in this study.

By estimating the fracture toughness of the SiC using nano-indentation, we revealed much smaller values than the typically cited values of approximately 3 MPa.m$^{1/2}$ for bulk SiC ceramics. Based on our previous evaluation of the fracture resistance on the friction surface of C_f/C-SiC composites, we anticipated that the fracture toughness of SiC region in these composites should have been less than 1.2 MP.m$^{1/2}$, in order to give a smaller fracture energy release rate than the Si. This is because in this study, physical cracks were seen extensively in the SiC regions, but not in the Si regions. Therefore, the estimated fracture toughness values generated by nano-indentation seem to support: (a) most of fracture toughness results from the database may not be suitable for assessing the resistance of micro-cracking in ceramics; (b) crack initiation resistance could be much smaller than the measured values from polycrystalline ceramics; (c) fracture toughness measurements by nano-indentation may be much closer to the crack initiation resistance, which should be useful for understanding any tribological related fracture damage.

In fact, the fracture resistance of polycrystalline ceramics could increase with crack extension, i.e. the well-known R-curve behaviour, whilst the magnitude of this increase could be in excess of a factor of three.[41] For ceramics with complex microstructures, like polycrystalline materials and composites, this difference would become more significant.[42] Therefore, in most cases, the measured fracture toughness values should be the maximum resistance of the crack propagation, which could only be reached after the cracks propagate with sufficient length. Support for this was gained from a study on the wear resistance of alumina, which revealed that the damage resistance had minimal relationship with any large crack propagation resistance, i.e. the fracture toughness measured by most methods.[43]

According to our earlier analysis,[16] the following possibilities may exist inside the SiC that might have led to its very low fracture initiation resistance: (a) the SiC regions in the composite might have been weakly bonded as the grain boundaries were not purposely engineered in the LSI process; (b) large residual tensile stresses may have existed on the grains boundaries or interfaces due to the constraint on the growth of the SiC grains during the LSI process in addition to the thermal strains generated during the cooling down period from the Si infiltration temperature, which are supported through the appearance of stacking fault inside the SiC grains.[44]

Unfortunately, under the current testing regime, it was unfeasible to initiate cracks in any of the carbon constituents. However, according to our previous estimation, their fracture toughness should be much smaller than the frequently quoted fracture toughness measured from C_f/C composites; this is likely where most of the fracture energy would be released by the interaction of the propagating cracks with a high level of microstructural features such as the interfaces in between the fibres and matrix.

5. Summary

Nano-indentation testing inside C_f/C-SiC composites demonstrated that both pyC formats, being either fibrous reinforcements or carbon matrices were subject to mechanical deformation behaviour similar to that of perfect elastic solids, regardless of the carbonaceous source. This elastic behaviour is supported by a linear relationship between the measured Young's modulus and hardness values from nano-indentation.

A difference of up to a factor of 2 in the Young's modulus and hardness were exhibited between PANOX carbon fibres that are used in most carbon/ceramic composites and high modulus AS4 carbon fibre typically used in carbon fibre reinforced plastic composites; this was also the case between the carbon matrix achieved through the CVI process and PIP of phenolic and epoxy resins. However, the measurements of these mechanical properties did not show a clear difference between carbon fibre reinforcements and pyC matrix in each composite.

Through an estimation of the upper (Voigit) and lower (Reuss) bounds of the Young's modulus for the pyC, it was shown that the measured Young's modulus values generated by the nano-indentation were near the Reuss bound of the estimation. If this is the case, variations in the measured Young's modulus are likely due to differences in the C_{44} elastic component of the graphite crystal, or an equivalent shear modulus of "clusters" in the carbon. However, it is clear that further study is needed for the true physical meaning of this proposed model.

Although there was no clear difference in the mechanical behaviour of the Si regions in all three of the composites, SiC produced from pyrolysed epoxy had an approximately 30% higher Young's modulus in comparison to those from pyrolysed methane or phenolic resin; this might be a result of different microstructure in SiC regions in each composite. The estimated values of fracture toughness by nano-indentation were in a range of 0.7–1.2 $MPa.m^{1/2}$ for SiC and ~0.6 $MPa.m^{1/2}$ for Si. It is believed these measurements represent the crack initiating resistance of a micro-fracture on a potential friction surface of these composite.

Acknowledgements

The authors would like to acknowledge the EPSRC (Grant Reference DT/E010938/1) and the Technology Strategy Board (TSB) in UK for their financial support that was used to conduct this research.

References

1. Naslain R. Design, preparation and properties of non-oxide CMCs for application in engines and nuclear reactors: an overview. *Compos Sci Technol* 2004;**64**:155–70.
2. Naslain R. SiC-matrix composites: nonbrittle ceramics for thermo structural application. *Int J Appl Ceram Technol* 2005;**2**:75–84.
3. Krenkel W, Berndt F. C/C-SiC composites for space applications and advanced friction systems. *Mater Sci Eng* 2005;**A412**:177–81.
4. Krenkel W. Cost effective processing of CMC composites by melt infiltration (LSI-process). *Ceram Eng Sci Proc* 2001;**23**:443–54.
5. Zhang Y, Xu Y, Lou J, Zhang L, Cheng L. Braking behavior of C/SiC composites prepared by chemical vapor infiltration. *Int J Appl Ceram Technol* 2005;**2**:114–21.
6. Zhao DL, Yin HF, Luo F, Zhou WC. Microstructure and mechanical properties of 3D textile C/SiC composites fabricated by chemical vapour infiltration. *Adv Mater Res* 2006;**11–12**:81–4.
7. Lin JM, Ma CCM, Tai NH, Wu WJ, Chen CY. Preparation and properties of SiC modified carbon–carbon composites by carbothermal reduction reaction. *J Mater Sci Lett* 1999;**18**:1353–5.
8. Li J, Tian J, Dong L. Synthesis of SiC precursors by a two-step sol–gel process and their conversion to SiC powders. *J Eur Ceram Soc* 2000;**20**:1853–7.
9. Muller E, Dittrich R, Moritz K. Studies on a novel route to C/SiC. *Adv Eng Mater* 2004;**6**:568–72.
10. Wu AH, Cao WB, Ge CC, Li JF, Kawasaki A. Fabrication and characteristics of plasma facing SiC-C functionally graded composite material. *Mater Chem Phys* 2005;**91**:545–50.
11. Ding Y, Dong S, Huang Z, Jiang D. Fabrication of short C fiber-reinforced SiC composites by spark plasma sintering. *Ceram Int* 2007;**33**:101–5.
12. Krenkel W. Design of ceramic brake pads and disks. *Ceram Eng Sci Proc* 2001;**23**:319–30.
13. Stadler Z, Krnel K, Kosmac T. Friction behaviour of sintered metallic brake pads on a C/C-SiC composite brake disc. *J Eur Ceram Soc* 2007;**27**:1411–7.
14. Fan SW, Xu YD, Zhang LT, Cheng LF, Yu L, Yuan YD, et al. Microstructure and properties of 3D needle-punched carbon/silicon carbide brake materials. *Compos Sci Technol* 2007;**67**:2390–8.
15. Xu Y, Zhang Y, Cheng L, Zhang L, Lou J, Zhang J. Preparation and friction behavior of carbon fiber reinforced silicon carbide matrix composites. *Ceram Int* 2007;**33**:439–45.
16. Wang Y, Wu H. Friction surface evolution of carbon fibre reinforced carbon/silicon carbide (C_f/C-SiC) composites. *J Eur Ceram Soc* 2010;**30**:3187–201.
17. Wu H, Wang Y. Friction silicon on carbon-fiber reinforced carbon-silicon Carbide (Cf/C-SiC). *High Temp Ceram Mater Comp* 2010:371–7.
18. Morgan P. *Carbon fibres and their composites*. Boca Raton: CRC Press; 2005.
19. Sawyer GR, Page TF. Microstructural characterization of "REFEL" (reaction-bonded) silicon carbides. *J Mater Sci* 1978;**13**:885–904.
20. Oliver WC, Pharr GM. An improved technique for determining hardness and elastic modulus using load and displacement sensing indentation experiments. *J Mater Res* 1992;**7**:1564–83.
21. VanLandingham MR. Review of instrumented indentation. *J Res Natl Inst Stand Technol* 2003;**108**:249–65.
22. Oliver WC, Pharr GM. Measurement of hardness and elastic modulus by instrumented indentation: advances in understanding and refinements to methodology. *J Mater Res* 2004;**19**:3–20.
23. Fischer-Cripps AC. Critical review analysis and interpretation of nanoindentation test data. *Surf Coat Technol* 2006;**200**:4153–65.
24. Fouquet S, Jouannigot S, Alexis J, Pailler R, Bourrat X, Guette A, et al. Nanoindentation, microscratch, friction and wear studies of carbon-fibre reinforced SiC-Si matrix composite. *Key Eng Mater* 2004;**264–268**:917–20.
25. Fouquet S, Rollin M, Pailler R, Bourrat X. Tribological behaviour of carbon fibres and ceramic matrix in the Si-C system. *Wear* 2007;**264**:850–6.
26. Evans AG, Charles EA. Fracture toughness determination by indentation. *J Am Ceram Soc* 1976;**59**:371–2.
27. Zhang T, Feng Y, Yang R, Jiang P. A method to determine fracture toughness using cube-corner indentation. *Scr Mater* 2010;**62**:199–201.
28. Lawn BR, Evans AG, Marshall DB. Elastic/plastic indentation damage in ceramics: the median/radial crack system. *J Am Ceram Soc* 1980;**63**:574–81.
29. Leatherbarrow A, Wu H. The development of the microstructure inside the carbon/silicon carbide composites manufactured by liquid silicon infiltration. *J Eur Ceram Soc* 2011.
30. Kutz M. *Handbook of materials selection*. New York: John Wiley & Sons; 2002.
31. Ma L, Sines G. Threshold size for cyclic fatigue crack propagation in a pyrolytic carbon. *Mater Lett* 1993;**17**:49–53.

32. Shackelford J, Alexander W. *Materials science & engineering handbook*. Boca Raton: CRC; 2000.
33. Hess P. Laser diagnostics of mechanical and elastic properties of silicon and carbon films. *Appl Surf Sci* 1996;**106**:429–33.
34. Berryman JG. Poroelastic shear modulus dependence on pore-fluid properties arising in a model of thin isotropic layers. *Geophys J Int* 2004;**157**:415–25.
35. Berryman JG. Bounds and self-consistent estimates for elastic constants of random polycrystals with hexagonal, trigonal, and tetragonal symmetries. *J Mech Phys Solids* 2004;**53**:2141–73.
36. Kelly BT. The elastic constants of polycrystalline carbons and graphites. *Philos Magn* 1964;**9**:721–37.
37. Seldin EJ, Nezbeda CW. Elastic constants of compression annealed pyrolytic graphite. *J Appl Phys* 1970;**41**:3373–82.
38. Northolt MG, Veldhuizen LH, Jansen H. Tensile deformation of carbon fibres and the relationship with the modulus for shear between the basal planes. *Carbon* 1991;**29**:1267–79.
39. Pharr GM, Bolshakov A. Understanding nanoindentation unloading curves. *J Mater Res* 2002;**17**:2660–71.
40. Ericson F, Johansson S, Schweitz JA. Hardness and fracture toughness of semiconducting materials studied by indentation and erosion techniques. *Mater Sci Eng* 1988;**A105–A106**:131–41.
41. Cook RF, Lawn BR, Fairbanks CJ. Microstructure-strength properties in ceramics: I effect of crack size on toughness. *J Am Ceram Soc* 1985;**68**:604–15.
42. Bennison SJ, Lawn BR. Role of interfacial grain-bridging sliding friction in the crack-resistance and strength properties of nontransforming ceramics. *Acta Metal* 1989;**37**:2659–71.
43. Cho SJ, Hockey BJ, Lawn BR, Bennison SJ. Grain-size and R-curve effects in the abrasive wear of alumina. *J Am Ceram Soc* 1989;**72**: 1249–52.
44. Leatherbarrow A, Wu H. The nature of silicon carbide phases developed from different carbonaceous sources and its impact on the microstructure of C_f/C-SiC composites. *Ceram Eng Sci Proc* 2010;**31**:73–83.